Available online at www.sciencedirect.com

ScienceDirect

journal homepage: www.elsevier.com/locate/he

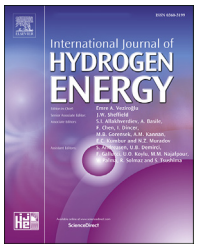

A discrete hidden Markov model fault diagnosis strategy based on K-means clustering dedicated to PEM fuel cell systems of tramways

Jiawei Liu [a], *Qi Li* [a,*], *Weirong Chen* [a], *Taiqiang Cao* [b]

[a] School of Electrical Engineering, Southwest Jiaotong University, Chengdu 611756, Sichuan Province, China
[b] School of Engineering and Electric Information, Xihua University, Chengdu 610039, Sichuan Province, China

ARTICLE INFO

Article history:
Received 1 October 2017
Received in revised form
11 April 2018
Accepted 22 April 2018
Available online 30 May 2018

Keywords:
Fuel cell tramways
Fault diagnosis
Discrete hidden Markov model
K-means clustering
Scalar quantization

ABSTRACT

To solve the fault classification problems of fuel cell (FC) various health states for tramways, a discrete hidden Markov model (DHMM) fault diagnosis strategy based on K-means clustering is proposed. In this paper, the K-means clustering algorithm is used to filter the sample points which aren't consistent with the actual class labels. The Lloyd algorithm is employed to quantify the sample vector sets and obtain the discrete code combination of training samples and test samples. The Baum-Welch algorithm and forward-backward algorithm are respectively presented to train and deduce the DHMM. The classification results show that the six concerned faults can be detected and isolated. The targeted fault types include low air pressure, deionized glycol high inlet temperature, deionized humidification pump low pressure, deionized glycol outlet temperature signal voltage overrange, normal state and hydrogen leakage. The fault recognition rates with the novel approach are at best 94.17%.

Introduction

Fuel cell converts the chemical energy of hydrogen and oxygen into electrical energy by electrochemical device [1–3]. It has the advantages of high energy conversion rate, low noise, fast dynamic response and modular design. It has broad prospects in distributed power generation, city tramways [4,5], city buses, electric vehicles and other transportation areas [6–8]. However, the fuel cell stack system (FCSS) is prone to malfunction in practical operation. The slight faults may cause reduction of output power and shutdown of stack. The serious failures can permanently damage the FC [9–11]. Therefore, fault detection and isolation (FDI) of fuel cell system has become one of the most important issues [12–14].

In recent years, artificial intelligence (AI) technologies have been widely used in the fault diagnosis of proton exchange membrane fuel cell (PEMFC) systems [15]. In Refs. [16,17], a cascade controller of the extended state observer (ESO) has been proposed for regulating the oxygen excess ratio of the PEMFC air-feed system to its desired value, based on the second-order sliding mode technique. The problem of fault diagnosis has been firstly considered in Ref. [18] for a class of nonlinear systems and successfully applied to a fuel cell air feed system. Lei Mao et al. [19,20] have proposed a novel sensor selection algorithm and its performance in PEMFC online diagnosis is investigated. The results show that the

* *Corresponding author.*
E-mail address: liqi0800@163.com (Q. Li).
https://doi.org/10.1016/j.ijhydene.2018.04.163

proposed algorithm can provide more efficient sensor selection results with less computational time. In Refs. [21,22], a general framework of fault diagnosis has been proposed to deal with multiple sensor measurements. Results show that features selected using singular value decomposition (SVD) can provide more effective classification results. E. Pahon et al. [23] have proposed a novel signal-based approach for fault diagnosis of PEMFC, which focuses on the detection of a high air stoichiometry (HAS) fault. The wavelet transform (WT) is used to diagnose quickly an oversupply of air to the PEMFC system. In order to describe the nonlinear voltage and current characteristics PEMFCs, D. Ritzberger et al. [24] have proposed a fault diagnosis method based on polynomial nonlinear autoregressive models with exogenous inputs (NARX) and the Volterra series. Ali Mohammadi et al. [25] have presented a 2 steps diagnosis approach for PEMFC. First, a 3D fault-sensitive model is built to simulate different faults (drying out and flooding) with 2 severity levels ("flooding", "drying", "high flooding" and "high drying"). Then, a two-layers feed-forward artificial neural network (ANN) has been developed to localize each fault in 9 considered segments within a single cell. The reservoir computing (RC) has been introduced into the field of FC diagnosis [26]. The targeted fault types include CO poisoning, low air flow rate, cooling circuit failure and system aging. Xingwang Zhao et al. [27] have proposed a fault diagnosis method based on multi-sensor signals and principal component analysis (PCA). The serious system fault and a single sensor failure have been successfully diagnosed and distinguished. Support vector machine (SVM) and designed diagnosis rules have been used to achieve FDI in real-time [28]. Four concerned failures have been diagnosed, including membrane drying, low air stoichiometry, low pressure fault and high pressure fault. The wavelet transform modulus maxima (WTMM) and pattern recognition methods have been combined to realize the fault diagnosis of PEMFC [29,30]. The continuous wavelet transform (CWT) and multifractal have been employed to calculate the singularity spectrum of the voltage signal. The SVM and K-nearest neighbor (KNN) algorithm have been used to classify the spectrum. The results show that the method can distinguish the faults such as cathode flow rate, gas pressure, cooling circuit and CO poisoning. The PEMFC electrochemical characteristic information has been extracted from the output terminal voltage signal (OTVS) by discrete wavelet decomposition [31]. Mona Ibrahima et al. [32] have presented discrete wavelet transform (DWT) to identify the membrane drying and flooding faults. The research shows that the DWT is more effective than the CWT in the field of fault diagnosis for fuel cell. Cédric Damour et al. [33] have proposed a novel empirical mode decomposition (EMD) based diagnosis approach dedicated to PEMFCs. The flooding and drying faults can be diagnosed by comparing the voltage contribution between the first and ninth intrinsic mode functions (IMFs). In order to find an online diagnostic tool for PEMFC, literature [34,35] have compared various types of PEMFC diagnostic methods in terms of diagnostic accuracy and computational complexity. PCA, Fisher discriminant analysis (FDA), kernel principal component analysis (KPCA) and kernel Fisher discriminant analysis (KFDA) have been used to extract features from the PEMFC voltage. Gaussian mixture model (GMM), KNN and SVM have been employed to make decisions. The experimental results show that the strategy based on FDA and SVM has higher performance and less computational cost than the other approaches.

However, most of the research work is focused on the small and medium size applications. The research on the fault diagnosis of the high power fuel cell system for the tramways is almost in the blank state. Electrochemical impedance spectroscopy (EIS) requires a high degree of professional knowledge with time-consuming and poor visibility. The kernel function of SVM is limited by the Mercer condition. The training time of relevant vector machine (RVM) increases rapidly with the increase of training samples. The sample size of neural network (NN) is large and easy to fall into "local minimum" and "over fitting". The fault samples can only be classified into several subclasses by clustering. The expert system has poor ability to acquire empirical knowledge and can't meet the requirements of real-time performance. The significant information may be lost with PCA.

Hidden Markov model (HMM) is a statistical modeling method for nonstationary time series [36,37]. It has the advantages of small training samples and interpretable feature. It can simultaneously reflect the randomness and latent structure of objects. It is applicable to modeling problems of complex dynamic nonlinear systems. HMM has been successfully used in many fields, such as network status analysis, state detection of electrical equipment, speech recognition and computer vision [38–41]. However, as far as we know, little literature studies the practical application of the Markov theory to identify the PEMFC faults. Bayesian-score (K2) and Markov chain Monte Carlo (MCMC) algorithms have been combined to construct the graphical-probability structure for fault diagnosis of FC [42]. Four types of faults in PEMFC are considered.

In this paper, a DHMM fault diagnosis strategy based on K-means clustering (DHMM-K) dedicated to PEM fuel cell systems of tramways is proposed for the first time. It has higher recognition accuracy and better expansibility for a variety of health states. The K-means clustering algorithm is used to eliminate singular sample points. The Lloyd method is employed to quantify the sample vector sets and obtain the discrete code combination of training samples and test samples. The Baum-Welch algorithm and the forward-back algorithm are respectively adopted to train and infer the DHMM. The experimental data from the tramway are proposed to verify the feasibility of the novel strategy. The advantages of the proposed approach are further proved by comparison with one-against-one (OAO) SVM.

Analysis of typical PEMFC faults for tramways

Fuel cell system structure in the tramway

FC/Super capacitor hybrid tramway is developed by Southwest Jiaotong University and CNR Tangshan Railway Vehicle Co., Ltd., as shown in Fig. 1. The configurations for the tramway have been listed in Table 1.

The detailed structure of PEMFC system has been shown in Fig. 2, which includes PEMFC subsystem, air supply subsystem and cooling cycle subsystem. The 150 kW Fcvelocity-HD6

Fig. 1 – The world's first hydrogen fuel cell/super capacitor hybrid tramway.

PEMFC stack of Ballard Power Systems Inc. is adopted as the fuel cell module. The configurations for the fuel cell stack have been listed in Table 2.

The schematic diagram of 150 kW PEMFC power generation system is shown in Fig. 3. The PEMFC subsystem consists FC stack, hydrogen circuit, air circuit and cooling circuit. The pressure relief valve and the pressure monitoring switch are distributed in the hydrogen storage module. The hydrogen enters the intake valve and the pressure sensor successively.

Table 2 – Configurations information for the fuel cell module.

Parameter	Value	Parameter	Value
Output voltage	465–730 V	Output current	20–320 A
Rated power	150 kW	Maximum power	170 kW
Net power output	110 kW	Cell number	735
Stack weight	404 kg	Coolant temperature	63 °C
Hydrogen pressure	16 barg	Air pressure	1.2 barg

The air circuit includes air filter, air compressor and mass flow controller (MFC). The circulation system of oil circuit is used for lubrication and heat dissipation of air compressor pump. The cooling circuit includes water pump, flow meter, water tank and radiator. The deionized coolant is used to achieve cooling with the heat of the oil circuit, the compressor motor and controller.

Safety classification of fuel cell systems for tramway

The fuel cell system of the tramway often fails in actual work. The slight faults can cause the system output power to decrease and stop. The serious failures may make the stack permanent damage and hydrogen explosion. Therefore, it is

Table 1 – Configurations information for the tramway.

Parameter	Value	Parameter	Value
Ambient temperature	−25–42 °C	Busbar voltage	750 V
Maximum operating speed	70 km h^{-1}	Axle load	10.5 t
Maximum slope	50‰	Train length	30.19 m
Train width	2.65 m	Train height	3.5 m
Passenger number	267	Train weight	51.06 t
Acceleration	1.2 m s^{-2}	Driving range	30 km
Wheel rolling radius	0.42 m	Windward area	7.28 m^2
Wind resistance coefficient	0.75	Mechanical transmission efficiency	0.97
Transmission ratio	6.0	Inertial mass coefficient	0.05

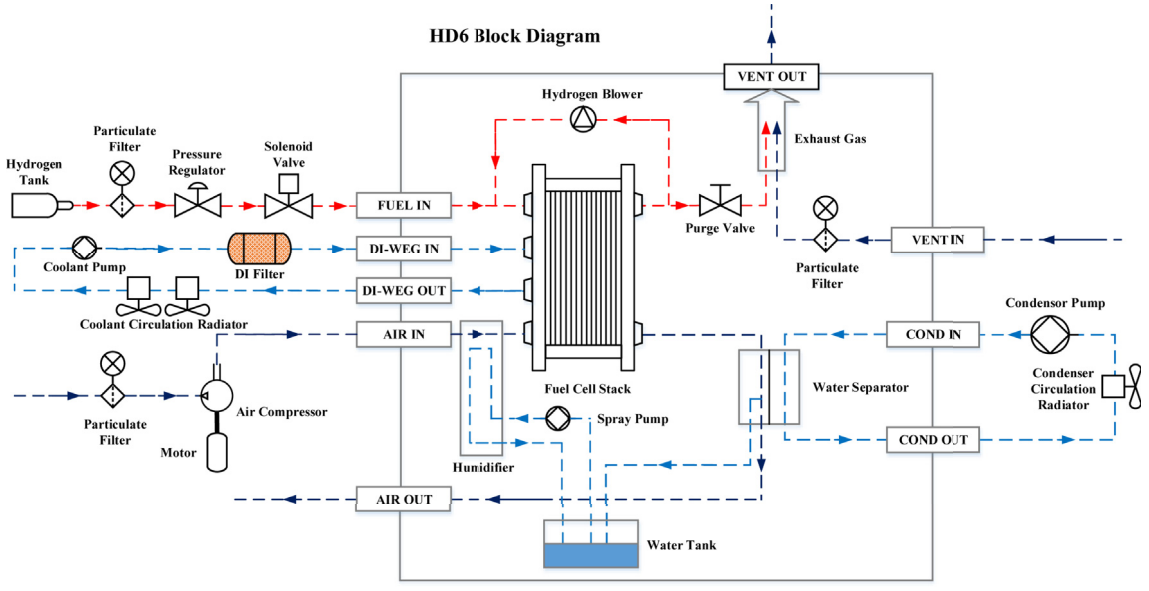

Fig. 2 – Schematic diagram of 150 kW fuel cell power generation system [4].

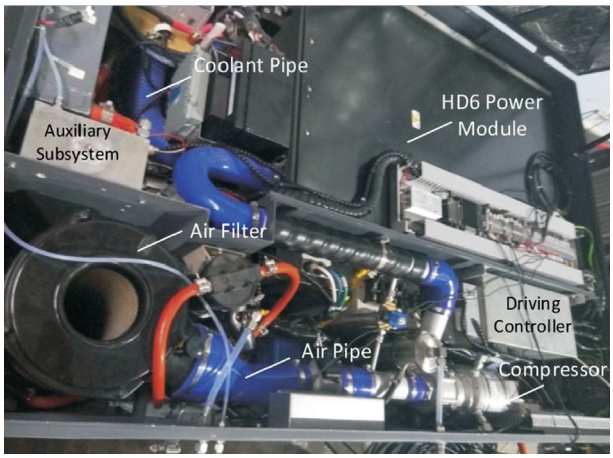

Fig. 3 – Physical map of the 150 kW PEMFC power generation system.

necessary to complete the fault classification from the point of view of safety and fault severity. The failures of the 150 kW Fcvelocity-HD6 fuel cell module are divided into four levels, defined as Table 3.

Level-0 alarm doesn't have any effect on the normal operation of the system. Level-1 alarm can reduce the output power of fuel cell module and can't cause the system to stop. The tramway is still operating under traction. If the level-1 alarm hasn't been immediately detected and isolated, the system will enter the level-2 (or level-3) alarm. If the system is in the level-2 (or level-3) state, the digital output of fuel cell module will switch to the fault state. The tramway immediately enters the shutdown mode and the fuel cell module stops working. The stack must be shut down immediately until the problem has been solved before restarting the fuel cell. This will seriously affect the safe operation of the tramway. Therefore, the detection and isolation of level-1 alarm can make the stack maintain the desired power operation and avoid system shut down. It is important to ensure the safe and stable running of tramway.

Considered faults

Based on the data extracted from the 150 kW PEMFC stack, the pie chart shown in Fig. 4 presents the percentage of most common PEMFC faults. Neglecting the aging effects of PEMFC, it is assumed that there is no components degradation of the tramway during the operation period. Failures include deionized glycol high inlet temperature, deionized humidification pump low pressure, deionized glycol outlet temperature signal voltage overrange, low air pressure and hydrogen leakage.

Hydrogen leakage

Hydrogen leakage means that there is not enough fuel to reach the PEMFC reaction site, which will directly reduce the output power level of the stack. When the concentration of hydrogen and oxygen is in [4%, 75%], hydrogen explosion may occur. The reasons for the hydrogen leakage include: blockage or leakage of hydrogen from the tank, the proton exchange membrane (PEM) breakage caused by too large differential pressure between the stack (or the single cell) anode and cathode, the fuel crossover. Specific leakage causes and corresponding repair methods are shown in Table 4.

Deionized humidification pump low pressure

The deionized humidification pump low pressure will reduce the relative humidity of the liquid water and the reacting gas. If the PEM isn't adequately humidified, drying fault may occur. Membrane drying will increase the ohm polarization and the internal resistance of FC, which result in lower output power. The causes of failure and methods of elimination are shown in Table 5.

Deionized glycol high inlet temperature

The deionized glycol high inlet temperature can raise the local temperature at the inlet end of the fuel cell stack, which leads to the nonuniform temperature distribution of the fuel cell stack. The PEM may be dehydrated and even damaged by the high temperature of the stack. The transmission rate of the proton can be affected. The deionized glycol high inlet temperature may reduce the conductivity and make the stack performance worse. Possible causes and methods of repair are shown in Table 6.

Deionized glycol outlet temperature signal voltage overrange

The temperature and pressure at the outlet end of the deionized coolant are monitored by the temperature and pressure sensors in real time. The inlet temperature of the coolant is controlled by the radiator fan and circulating water pump. The temperature sensor at the outlet end of the stack may be damaged by the deionized glycol outlet temperature signal voltage overrange. The coolant temperature at the

Table 3 – Safety classification of fuel cell system for tramway.

Security level	Description
Level-0 alarm	No reporting to drive system, no system reaction. For information only.
Level-1 alarm	A system parameter has exceeded normal range. Fuel cell module (FCM) output power may be reduced while the fault is active. Doesn't result in a shutdown.
Level-2 alarm	A system parameter has exceeded acceptable operating range, and the fuel cell module will shut down. Once measured current has dropped to 0, the FCM will switch to standby state, then to faulted state. If a level-2 fault has been active for more than 10 s, the FCM will immediately enter faulted state.
Level-3 alarm	A system parameter has exceeded a safe operating range, and the fuel cell module must be immediately shut down. The FCM will immediately enter faulted state. After a level-3 fault, the fuel cell module mustn't be restarted until the cause of the fault has been determined and resolved. In addition, the module should be inspected for safe operation.

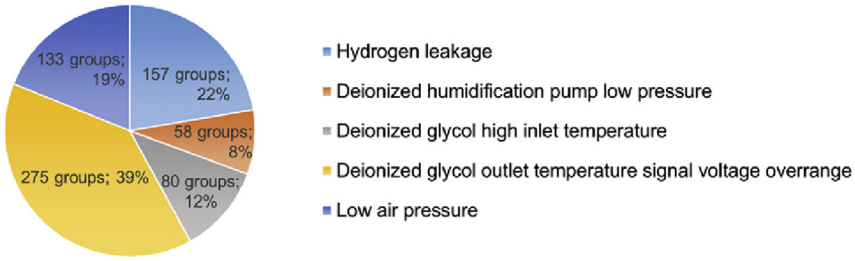

Fig. 4 – Fault percentage of level-1 alarm of fuel cell system.

outlet end of the stack will get out of control and result in thermal management system failure. The performance of the stack may be damaged and the service life can be shortened by FC internal short-term high temperature. The cause of failure and the elimination methods are shown in Table 7.

Low air pressure

The air pressure is the result of the continuous accumulation of cathode oxygen flow. The low internal air flow of the stack can cause insufficient oxygen supply. When the air excess coefficient is too low, there may be "oxygen starvation" failure. The output voltage of the stack will be greatly attenuated and the voltage uniformity will be severely damaged. The single cell with the lowest voltage is close to the state of limit current density. The surface of the PEM appears "hot spot" and even burns, which may shorten the service life of the stack. The possible causes and maintenance measures are shown in Table 8.

Table 4 – Troubleshooting sheet of hydrogen leakage.

Possible causes	Repair method
Hydrogen sensor is out of calibration	Check hydrogen sensor
Faulty purge valve	Check purge valve operation
The air system can't start up	Check air system operation
Hydrogen internal transfer leak in fuel cell	Perform module transfer leak test
Pressure relief valve is not sealed properly	Perform module transfer leak test
Faulty hydrogen sensor or wiring issue	Check hydrogen sensor functionality and wiring
Actual hydrogen leak within the FC module (fuel cells, hose, piping, etc.)	Perform module external leak test
Hydrogen sensor mounting block leakage in ventilation box	Check mounting block seal integrity.
Module ventilation filter blockage	Inspect module ventilation filter
Insufficient air ventilation of module	Check ventilation operation

Table 5 – Troubleshooting sheet of deionized humidification pump low pressure.

Possible causes	Repair method
Spray water tank is empty	Fill spray water tank
Air in spray water pump	Adjust spray water tank level
Spray water circuit severe leak	Inspect spray water circuit for leakage
Spray water pump malfunction	Check spray water pump operation
Spray water particulate filter blockage	Inspect particulate filter
Spray water pump is worn out	Rebuild spray water pump
Faulty pressure sensor or wiring issue	Check pressure sensor functionality and wiring
Spray water system leakage	Inspect spray water system
Fuel cell module condenser malfunction	Inspect condenser system for proper flow and temperature
Too low air inlet pressure of fuel cell module	Inspect air system (air compressor, air by-pass valve(s), air back pressure valve(s))

Table 6 – Troubleshooting sheet of deionized glycol high inlet temperature.

Possible causes	Repair method
Air in cooling system of fuel cell module	Check coolant bleed port, de-air cooling system
Cooling system malfunction (heater, heat exchanger, etc)	Check cooling system operation
Faulty pressure sensor or wiring issue	Check pressure sensor functionality and wiring
Coolant into stack is above temperature specification	Check coolant system operation
Coolant heater system malfunction	Check coolant heater system operation
Faulty temperature sensor or wiring issue	Check temperature sensor functionality and wiring

Table 7 – Troubleshooting sheet of deionized glycol outlet temperature signal voltage overrange.

Possible causes	Repair method
Faulty pressure sensor or wiring issue	Check pressure sensor functionality and wiring
Faulty temperature sensor or wiring issue	Check temperature sensor functionality and wiring

Table 8 – Troubleshooting sheet of low air pressure.

Possible causes	Repair method
Module air supply system malfunction	Check air supply system operation
Module back pressure valve malfunction	Check back pressure valve setting and operation
Air by-pass valve malfunction	Check air by-pass valve operation
Module air exhaust blockage	Check air exhaust for blockage
Faulty temperature sensor or wiring issue	Check temperature sensor functionality and wiring

DHMM-K

In this paper, a novel fault diagnosis model of fuel cell system for tramway is constructed by combining DHMM and K-means clustering. The establishment process of DHMM and K-means clustering is introduced as follows:

The principle and algorithm of DHMM

Principle of DHMM

DHMM is a state classifier with timing recognition capability and usually described by five elements, namely $\lambda = (N, M, \pi, A, B)$. The specific parameters are defined as follows [41]:

(1) The state number of the Markov chain in the model is N.

The state is denoted by $S = \{S_1, S_2, \cdots, S_N\}$, where the state at time t is q_t.

(2) The number of observations in the hidden state is M.

The state of the observation corresponds to the physical output of the system. These states are denoted as $V = \{v_1, v_2, \cdots, v_M\}$.

(3) Initial state probability vector is $\Pi = \{\pi_i\}$.

$$\pi_i = P(q_1 = S_i), 1 \le i \le N, \sum_{i=1}^{N} \pi_i = 1 \quad (1)$$

π_i indicates the probability that the initial state is S_i.

(4) State transition probability matrix is $A = \{a_{ij}\}$.

$$a_{ij} = P(q_{t+1} = S_j | q_t = S_i), 1 \le i, j \le N, \sum_{j=1}^{N} a_{ij} = 1 \quad (2)$$

a_{ij} is the transition probability from state S_i to state S_j.

(5) Observation probability matrix is $B = \{b_j(k)\}$.

$$b_j(k) = P(O_t = v_k | q_t = S_j), 1 \le j \le N, 1 \le k \le M, \sum_{k=1}^{M} b_j(k) = 1 \quad (3)$$

$b_j(k)$ represents the observed probability distribution at state j.

The hidden Markov model is divided into two parts: one is the hidden Markov chain where the state sequence is formed by the combination of π and A; the other is a random process that can be directly observed and the sequence of observations is output by B. The composition of DHMM is shown in Fig. 5, where T is the time length of the observed sequence.

The Markov chain structure of the six-state DHMM is shown in Fig. 6. $S_i (i = 1, 2, \cdots, 6)$ characterizes the ith state of the Markov chain. $a_{ij} (i, j = 1, 2, \cdots, 6)$ represents the state transition probability from state S_i to state S_j.

Algorithm of DHMM

In order to apply DHMM to practical systems, three key problems (i.e. probability estimation, optimal state sequence and parameter estimation) are needed to be solved. The corresponding effective mathematical methods are as follows [36,43]:

(1) Forward-backward algorithm

Observation sequence $O = \{O_1, O_2, \cdots, O_T\}$ and model λ are known. $P(O|\lambda)$ is needed to be solved.

Define the forward variable as:

$$\alpha_t = P(O_1, O_2, \cdots, O_t, q_t = S_i | \lambda), 1 \le t \le T \quad (4)$$

Initialization:

$$\alpha_1(i) = \pi_i b_i(O_1) \quad (5)$$

Recursion:

$$\alpha_{t+1}(i) = \left[\sum_{i=1}^{N} \alpha_t(i) a_{ij}\right] b_j(o_{t+1}), 1 \le t \le T, 1 \le j \le N \quad (6)$$

Termination:

$$P(O|\lambda) = \sum_{i=1}^{N} \alpha_T(i) \quad (7)$$

The forward probability is calculated in the two steps of initialization and recursion, namely the joint probability of the

Fig. 5 – Composition diagram of DHMM.

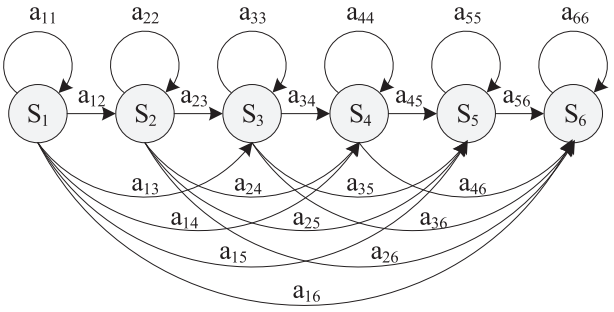

Fig. 6 – Six-state DHMM

hidden state and the initial observation. The sum of the final forward variables is used as the value of the $P(O|\lambda)$ in the last step.

Similarly, the definition of the backward variable is:

$$\beta_t = P(O_{t+1}, O_{t+2}, \ldots, O_T, q_t = S_i|\lambda), 1 \le t \le T-1 \tag{8}$$

Initialization:

$$\beta_T(i) = 1, 1 \le i \le N \tag{9}$$

Recursion:

$$\beta_t(i) = \sum_{j=1}^{N} \alpha_{ij} b_j(O_{t+1}) \beta_{t+1}(j), 1 \le t \le T-1, 1 \le i \le N \tag{10}$$

Termination:

$$P(O|\lambda) = \sum_{i=1}^{N} \beta_t(i) \tag{11}$$

(2) Viterbi algorithm

Observation sequence $O = \{O_1, O_2, \cdots, O_T\}$ and model λ are known. The most likely state sequence $q = \{q_1, q_2, \cdots, q_T\}$ is needed to be found [38,44].

The maximum probability of the state sequence $O_1, O_2, \cdots, O_t$ is defined as $\delta_t(i)$, where the path is $q_1, q_2, \cdots, q_t$ and $q_t = S_i$.

$$\delta_t(i) = \max_{q_1, q_2, \ldots, q_{t-1}} P(q_1, q_2, \ldots, q_t = S_i, O_1, O_2, \ldots, O_t|\lambda) \tag{12}$$

The procedure for finding the optimal state sequence is as follows:

Initialization:

$$\delta_1(i) = \pi_i b_i(O_1), 1 \le i \le N \tag{13}$$

$$\varphi_1(i) = 0, 1 \le i \le N \tag{14}$$

Recursion:

$$\delta_t(i) = \max_{1 \le i \le N} \left([\delta_{t-1}(i) a_{ij}] \right) b_j(O_t), 2 \le t \le T, 1 \le j \le N \tag{15}$$

$$\varphi_t(j) = \operatorname*{argmax}_{1 \le i \le N} [\delta_{t-1}(i) a_{ij}], 1 \le t \le T, 1 \le j \le N \tag{16}$$

Termination:

$$P^* = \max_{1 \le i \le N} [\delta_T(i)] \tag{17}$$

$$q_T^* = \operatorname*{argmax}_{1 \le i \le N} [\delta_T(i)] \tag{18}$$

(3) Baum-Welch algorithm

Observation sequence $O = \{O_1, O_2, \cdots, O_T\}$ and initial conditions are known. The most likely state sequence $q = \{q_1, q_2, \cdots, q_T\}$ is needed to be found. Make $P(O|\lambda)$ maximum by adjusting the model parameter $\lambda = (\pi, A, B)$ [37,45].

Define two variables:

$$\xi_t(i,j) = P(q_t = s_i, q_{t+1} = s_j|O, \lambda) \tag{19}$$

$$\gamma_t(i) = P(q_t = s_i||O, \lambda) \tag{20}$$

According to the definition of forward and backward variables:

$$\xi_t(i,j) = \frac{\alpha_t(i) a_{ij} b_j(O_{t+1}) \beta_{t+1}(j)}{P(O|\lambda)} = \frac{\alpha_t(i) a_{ij} b_j(O_{t+1}) \beta_{t+1}(j)}{\sum_{i=1}^{N} \sum_{j=1}^{N} \alpha_t(i) a_{ij} b_j(O_{t+1}) \beta_{t+1}(j)} \tag{21}$$

$$\gamma_t(i) = \sum_{j=1}^{N} \xi_t(i,j) \tag{22}$$

The formula of parameter revaluation is derived from the maximum likelihood principle:

$$\overline{\pi}_i = \gamma_1(i) \tag{23}$$

$$\overline{a_{ij}} = \frac{\sum_{t=1}^{T-1} \xi_t(i,j)}{\sum_{t=1}^{T-1} \gamma_t(i)} \tag{24}$$

$$\overline{b_j}(k) = \frac{\sum_{t=1}^{T} \gamma_t(j)}{\sum_{t=1}^{T} \gamma_t(j)} \tag{25}$$

According to the observation sequence O and the initial model $\lambda_0 = (\pi, A, B)$, in order to obtain the trained parameter $\overline{\lambda} = (\overline{\pi}, \overline{A}, \overline{B})$, the recursive formulas (23)–(25) are used to calculate repeatedly until $P(O|\overline{\lambda})$ converges.

K-means clustering

The K-means clustering algorithm is a well-known division clustering segmentation method [46–49]. K points are randomly selected from the datasets as the initial clustering center. The Euclidean distance from each sample to the cluster center is calculated. The sample is returned to the nearest cluster center [50–52]. The new clustering center is obtained by calculating the average value of the newly formed data objects of each cluster. If there is no change in the two adjacent clusters, it shows that the sample adjustment is over and the clustering criterion function has been converged.

The European distance of sample $x = (x_1, x_2, \cdots, x_n)$ and initial cluster center $z = (z_1, z_2, \cdots, z_n)$ are denoted by $d(x_i, z_i)$:

$$d(x,z)=\left[\sum_{i=1}^{n}(x_i,z_i)^2\right]^{\frac{1}{2}} \tag{26}$$

The sum of within-class distance J is used as the evaluation function of clustering quality:

$$J=\sum_{j=1}^{k}\sum_{i=1}^{n_j}d(x_i,z_j),x_i=C_j \tag{27}$$

Among them: n_j is the sample size of subclass C_j; z_j is the clustering center of subclass C_j, $d(x_i,z_j)$ is the distance between sample x_i and cluster center z_j; J is the sum of all with-class distances. The smaller the value of J, the better the clustering effect. The algorithm flow chat is shown in Fig. 7.

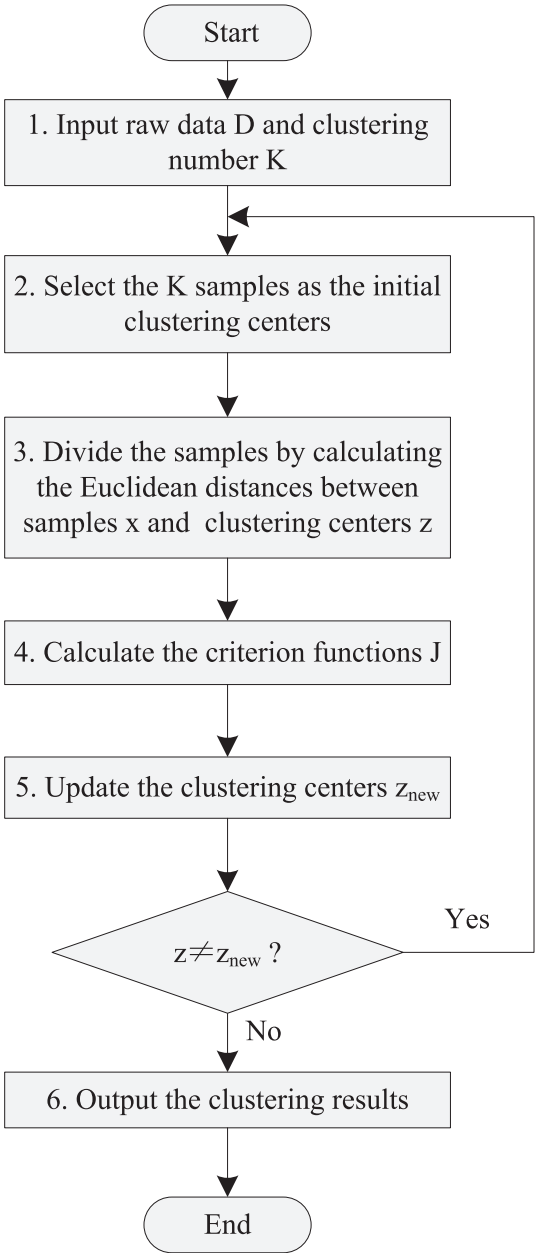

Fig. 7 – Flow chart of K-means clustering algorithm.

Fault diagnosis procedure of PEMFC

The fault diagnosis procedure of the novel method can be divided into two stages: model training and fault classification.

The implementation steps of model training phase are as follows:

(1) The fault data of the tramway operation are selected as the original datasets;
(2) The properties that can directly reflect the running state of the fuel cell systems are selected as the diagnostic variables;
(3) The fault characteristic data are normalized;
(4) The K-means clustering algorithm is used to eliminate the sample points that don't match the actual class labels;
(5) The Lloyd algorithm is used to convert the datasets into discrete codebook index sequences;
(6) The Baum-Welch algorithm is used to establish the DHMMs corresponding to the various fault states of the fuel cell systems for tramways.

The implementation steps of fault classification phase are as follows:

(1) According to the steps (1)–(5) of the model training stage, the unknown fault datasets are input and the features are extracted to obtain the observation sequence;
(2) The observation sequence is sent to each discrete hidden Markovian diagnostic model. The forward-backward algorithm is used to calculate the probability of the observation sequence in each model;
(3) The model with the maximum probability of output is taken as the model corresponding to the observation sequence. The corresponding fault type is the health state of the current observation sequence.

Fault classification flowchart of DHMM-K is shown in Fig. 8.

Example analysis of fault diagnosis

Example description

Through the experimental test of tramway, the relevant measured data are taken as the original datasets. The 800 sets of experimental data of the 150 kW fuel cell No. 1 stack are selected as the original datasets. There are six kinds of health states, including normal state 93 groups, hydrogen leakage 157 groups, deionized humidification pump low pressure 58 groups, deionized glycol high inlet temperature 80 groups, deionized glycol outlet temperature signal voltage overrange 275 groups, low air pressure of 133 groups.

Fault feature vector extraction

Thirteen important signals that directly reflect the operation states of the FCSS are chosen as the feature vectors. The symbol description of thirteen parameters has been listed in

Table 9. The feature vectors are normalized and values of each attribute are limited to the range of [0, 1].

K-means clustering and filtering

In order to improve the accuracy of the fault diagnosis algorithm, the samples are needed to be filtered. The K-means algorithm is used to cluster the 800 normalized data and exclude sample points that don't match the actual class labels. For each health state, 50 sets of data are selected as sample feature vector sets, in which the first 30 groups are used to train the model and the latter 20 groups are used as test datasets.

Training and identification of DHMM

The fault diagnosis process is divided into training phase and test phase. Firstly, the Lloyd algorithm is used to quantize the sample feature vectors. The discrete coded combination of training samples and test samples is obtained. The maximum quantization codeword is set to 8 and the minimum codeword is 1. That is the code level is 8. Then, state transition probability matrix of the training samples of the *ith* $(i = 1, 2, \cdots, 6)$ class health state is input and the model parameters of the *ith* class fault are trained. Finally, the observation sequences of the samples to be identified are input and the probability value

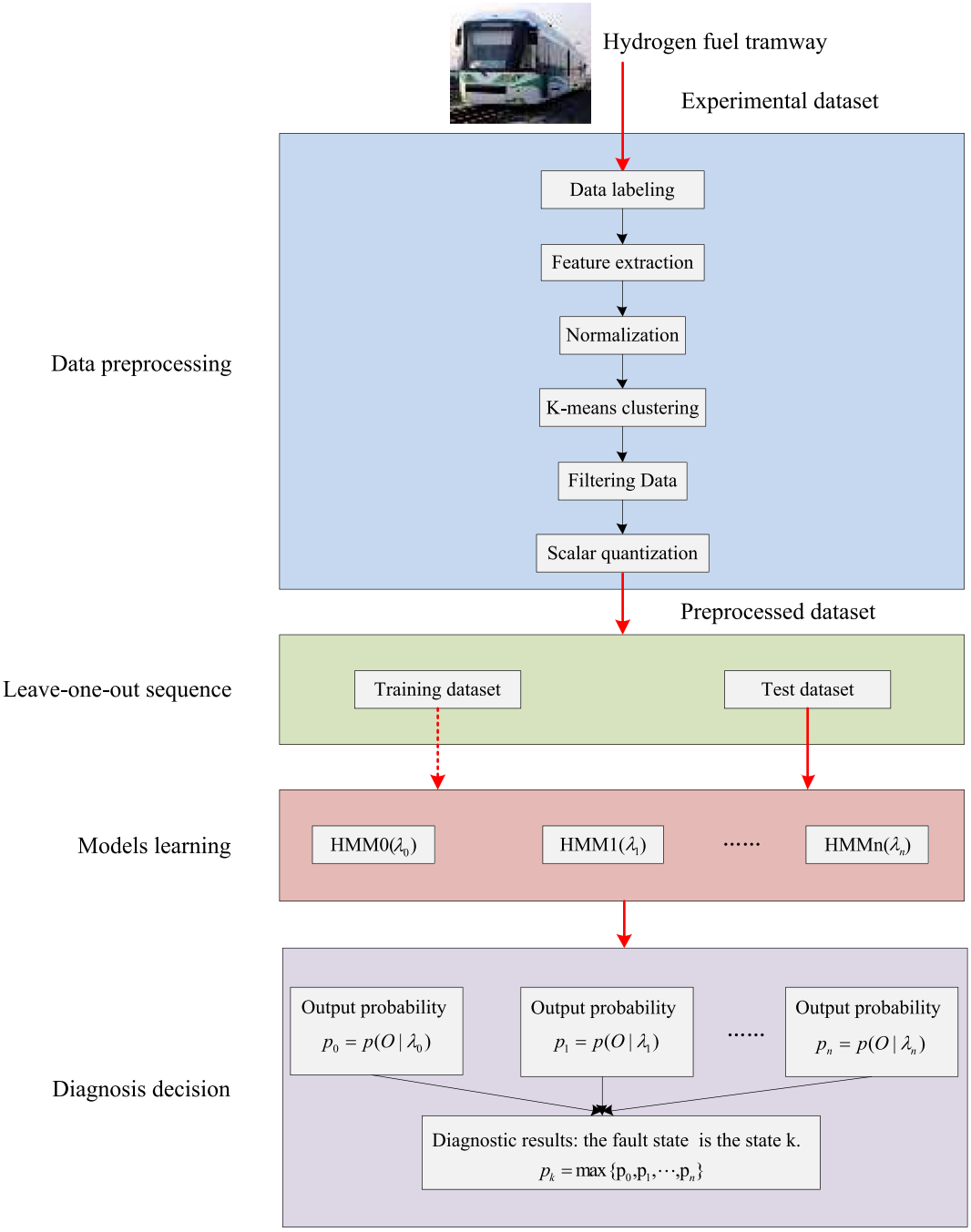

Fig. 8 – Flow chart of fault classification procedures.

Table 9 – Variables of FCSS.

Diagnostic variable	Symbol
Stack output hydrogen pressure	$P_{Hsk\ out}$
Stack input hydrogen pressure	$P_{Hsk\ in}$
Coolant inlet pressure	$P_{co\ in}$
Air inlet pressure	$P_{air\ in}$
Stack coolant outlet temperature	$T_{water\ out}$
Stack coolant inlet temperature	$T_{water\ in}$
Inlet air temperature of air compressor	$T_{Acair\ in}$
Air outlet temperature	$P_{air\ out}$
Module inlet hydrogen pressure	$P_{Hmo\ in}$
Module coolant inlet temperature	$T_{Mowater\ in}$
Stack current	I_{total}
Stack voltage	V_{total}
Hydrogen pressure	P_H

of the sequences are calculated for each DHMM. The model number corresponding to the maximum probability is the fault type.

Classification results

In this paper, the number of DHMMs is Q = 12 and the number of observations is O = 8. The number of observations is equal to the code level. When the DHMM is used to classify the faults, it is found that the code size has a great influence on the recognition rate. If the code level is too small, the classification accuracy will be greatly reduced. If the code level is too large, the recognition rate will decrease and the computational complexity will increase significantly. Therefore, this paper chooses the code level of 8, which can ensure the

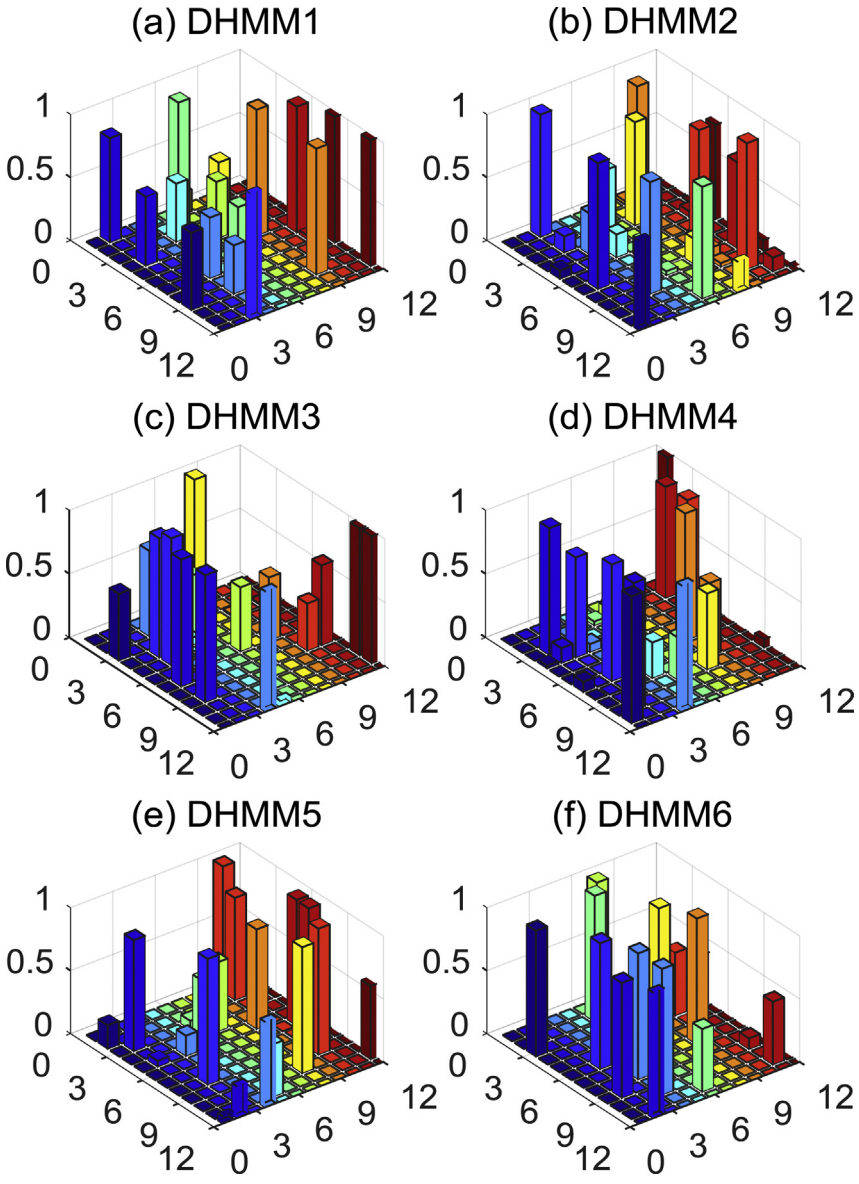

Fig. 9 – State transition matrix of DHMM.

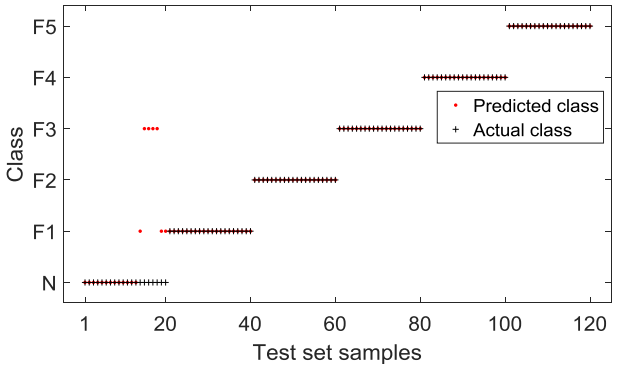

Fig. 10 – Classification results of the training data.

recognition accuracy without increasing the computational cost. The state transition probability matrix after training is shown in Fig. 9.

The classification results of six kinds of fault test samples are shown in Fig. 10. The statistical results are shown in Table 10.

According to the analysis of Table 10, the fault diagnosis method of DHMM-K has a good classification ability. The average recognition rate is 94.17%. The classification accuracy of normal state is 65%, the recognition rate of the other five kinds of faults are 100%. A total of 7 sets of normal state are misdiagnosed. Among them, three groups of normal state are incorrectly diagnosed as hydrogen leakage, four groups of normal state are wrongly diagnosed as deionized glycol high inlet temperature.

Fault diagnosis method based on SVM

Based on the principle of statistical theory and structural disorientated minimization (SRM), SVM has the characteristics of fast learning speed, high prediction precision, powerful non-linear system modeling capability and suitability for small samples [28,53].

In this paper, thirteen important signals regarding all the subsystems of FCSS are directly reflected as the feature vectors of fault diagnosis. 300 groups of PEMFC samples are gathered from the 715 single cells to set up the SVM model. The datasets contain six types of PEMFC states. 180 samples are randomly selected to train the model, and the left 120 data are employed to test the SVM model. The 180 samples are comprised of 30 low air pressure samples, 30 deionized glycol high inlet temperature samples, 30 deionized humidification pump low pressure samples, 30 deionized glycol outlet temperature signal voltage overrange samples, 30 normal states samples and 30 hydrogen leakage samples. The 120 test samples include 20 samples of low air pressure, 20 samples of deionized glycol high inlet temperature, 20 samples of low pressure of deionized humidification pump low pressure, 20 samples of deionized glycol outlet temperature signal voltage overrange, 20 samples of normal states and 20 samples of hydrogen leakage.

The penalty parameter c and kernel function parameter g have great influences on the SVM performance. In this paper, 5-fold cross-validation is employed to determine the appropriate values of the regularization factor and kernel function width. In the cross-validation, the SVM training datasets is

Table 10 – Statistical results of classified diagnosis of test data.

Fault type	Number of samples	Recognition result		Recognition rate
		Correct	Error	
Normal state	20	13	7	65%
Hydrogen leakage	20	20	0	100%
Deionized humidification pump low pressure	20	20	0	100%
Deionized glycol high inlet temperature	20	20	0	100%
Deionized glycol outlet temperature signal voltage overrange	20	20	0	100%
Low air pressure	20	20	0	100%
Total	120	113	7	94.17%

randomly split into 5 exclusive subsets of approximately equal size. The holdout method is repeated 5 times, and then the average error across all 5 trials is calculated. The best parameters obtained for the SVM classifier are $g = 2$ and $c = 0.35$, which incur a training accuracy of 98.33%. The diagram of parameter selection for the PEMFC training samples are given in Fig. 11.

A fault diagnosis strategy based on the combination of one-against-one SVM and fault degree is used to realize fault diagnosis and isolation [27,33]. The classification results of test set are shown in Fig. 12. The fault diagnosis results are shown in Table 11. The average recognition rate is 87.5%. The classification accuracy of normal state and hydrogen leakage are 75%. The recognition rate of deionized humidification pump low pressure and deionized glycol high inlet temperature are 95%. The error diagnosis rate (EDR) of low air pressure is 15%. The classification accuracy of deionized glycol outlet temperature signal voltage overrange is 100%.

Comparison and analysis of algorithms

The algorithms are run under a computer with a CORE i7-7700HQ and 8G DDR4 RAM. As in Table 12, different methodologies are evaluated from the perspectives of occupied memory and computation time. The classification accuracy of

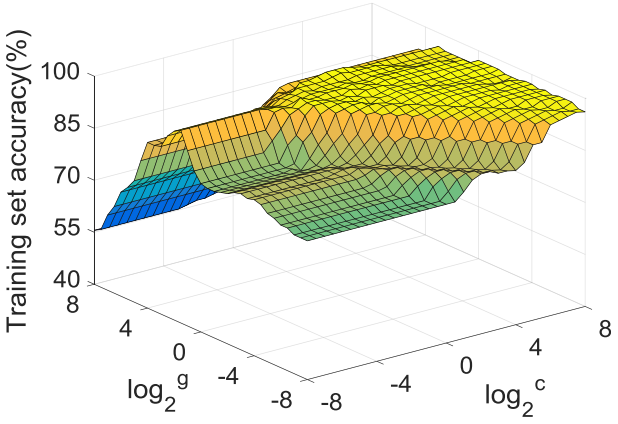

Fig. 11 – Diagram of parameter selection.

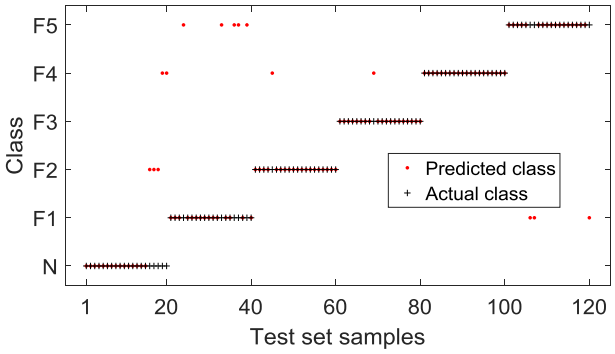

Fig. 12 – Classification results of the test data of SVM.

Table 11 – Fault diagnosis result of SVM.

Fault type	Number of samples	Recognition result		Recognition rate
		Correct	Error	
Normal state	20	15	5	75%
Hydrogen leakage	20	15	5	75%
Deionized humidification pump low pressure	20	19	1	95%
Deionized glycol high inlet temperature	20	19	1	95%
Deionized glycol outlet temperature signal voltage overrange	20	20	0	100%
Low air pressure	20	17	3	85%
Total	120	105	15	87.5%

Table 12 – Computation time and accuracy of the algorithm.

Algorithm	DHMM-K	SVM
Computation time/s	1.48	9.06
Accuracy/%	94.17%	87.5%

the novel method is 94.17%, which is higher than SVM for the six kinds of health states for the tramway. It shows that the novel method has higher recognition accuracy. Apart from classification accuracy, computation cost is a crucial factor that needs to be taken into account. The computation time is here used to describe the computation cost. The computational time of the proposed method is 1.48 s, which is much lower than SVM. It shows that the computational cost of the proposed method is less than that of SVM.

From this table, it can be seen that compared with the SVM method, occupied memory and computation time of the novel method are small. Hence, considering synthetically the performances of EDR and feasibility of online implementation, the fault diagnosis strategy of DHMM-K can be chosen as final solution in our case [34].

Conclusion

In this paper, the fault diagnosis strategy of DHMM-K is proposed. K-means clustering algorithm is adopted to eliminate the sample points which aren't consistent with the actual class labels. Lloyd algorithm is used to quantify the sample feature. Baum-Welch algorithm and forward-backward algorithm are presented to train and infer the DHMM. According to the measured data of the tramway, the average recognition rate of the six fault samples is 94.17%. The results prove the effectiveness of the method in the fault diagnosis of the fuel cell systems for the tramways. Compared with the SVM method, the DHMM-K method has the advantages of small computation cost, high classification accuracy and easy expansion. When a new fault type occurs, only new samples are trained to generate a hidden Markov model with good scalability. The DHMM-K strategy has low computational complexity and is suitable for small sample data. It lays an important foundation for the on-line fault diagnosis of the fuel cell system for the tramways.

At present, the work of coding the strategy in an embedded microprocessor chip and online testing is in process. Additionally, to recognize unknown fault types, some effort is being made to improve the current approach.

Acknowledgments

This work was supported by National Natural Science Foundation of China (61473238), Scientific Funds for Outstanding Young Scientists of Sichuan Province of China (2015JQ0016), NEEC Open-end Fund of China (NEEC-2017-B01).

REFERENCES

[1] Hong Ling, Chen Jian, Liu Zhiyang, Huang Lianghui, Wu Zhongle. A nonlinear control strategy for fuel delivery in PEM fuel cells considering nitrogen permeation. Int J Hydrogen Energy 2017;42:1565–76.
[2] Li Qi, Yang Hanqing, Han Ying, Li Ming, Chen Weirong. A state machine strategy based on droop control for an energy management system of PEMFC-battery-supercapacitor hybrid tramway. Int J Hydrogen Energy 2016;41:16148–59.
[3] Liu Jianxing, Laghrouche Salah, Ahmed Fayez-Shakil, Wack Maxime. PEM fuel cell air-feed system observer design for automotive applications: an adaptive numerical differentiation approach. Int J Hydrogen Energy 2014;39:17210–21.
[4] Li Qi, Chen Weirong, Liu Zhixiang, Li Ming, Ma Lei. Development of energy management system based on a power sharing strategy for a fuel cell-battery-supercapacitor hybrid tramway. J Power Sources 2015;279:267–80.
[5] Li Qi, Chen Weirong, Liu Zhixiang, Guo Ai, Huang Jin. Nonlinear multivariable modeling of locomotive proton exchange membrane fuel cell system. Int J Hydrogen Energy 2014;39:13777–86.
[6] Xie Changjun, Ogden Joan M, Quan Shuhai, Chen Qihong. Optimal power management for fuel cell–battery full hybrid powertrain on a test station. Int J Electr Power 2013;53:307–20.
[7] Jia Junbo, Wang Gucheng, Thean Cham Yew, Wang Youyi, Han Ming. Electrical characteristic study of a hybrid PEMFC and ultracapacitor system. IEEE Trans Ind Electron 2010;57:1945–53.
[8] Xie Changjun, Xu Xinyi, Bujlo Piotr, Shen Di, Zhao Hengbing, Quan Shuhai. Fuel cell and lithium iron phosphate battery

hybrid powertrain with an ultracapacitor bank using direct parallel structure. J Power Sources 2015;279:487–94.
[9] Benmouna A, Becherif M, Depernet D, Gustin F, Ramadan HS. Fault diagnosis methods for proton exchange membrane fuel cell system. Int J Hydrogen Energy 2017;42:1534–43.
[10] Sutharssan T, Montalvao D, Chen YK, Wang WC, Pisac C. A review on prognostics and health monitoring of proton exchange membrane fuel cell. Renew Sustain Energy Rev 2017;75:440–50.
[11] Dijoux E, Steiner NY, Benne M, Péra M, Pérez BG. A review of fault tolerant control strategies applied to proton exchange membrane fuel cell systems. J Power Sources 2017;359:119–33.
[12] Hissel D, Pera MC. Diagnostic & health management of fuel cell systems: issues and solutions. Annu Rev Control 2016;42:201–11.
[13] Liu J, Wu C, Wang Z, Wu L. Reliable filter design for sensor networks using type-2 Fuzzy framework. IEEE Trans Ind Inform 2017;13:1742–52.
[14] Andújar JM, Segura F, Isorna F, Calderón AJ. Comprehensive diagnosis methodology for faults detection and identification, and performance improvement of air-cooled polymer electrolyte fuel cells. Renew Sustain Energy Rev 2018;88:193–207.
[15] Zhao Y, Shen Y, Bernard A, Cachard C, Liebgott H. Evaluation and comparison of current biopsy needle localization and tracking methods using 3D ultrasound. Ultrasonics 2017;73:206–20.
[16] Liu J, Gao Y, Su X, Wack M, Wu L. Disturbance-observer-based control for air management of PEM fuel cell systems via sliding mode technique. IEEE Trans Control Syst Technol 2018:1–10.
[17] Wu L, Gao Y, Liu J, Li H. Event-triggered sliding mode control of stochastic systems via output feedback. Automatica 2017;82:79–92.
[18] Liu Jianxing, Luo Wensheng, Yang Xiaozhan, Wu Ligang. Robust model-based fault diagnosis for PEM fuel cell air-feed system. IEEE Trans Ind Electron 2016;65:3261–9.
[19] Mao L, Jackson L, Davies B. Effectiveness of a novel sensor selection algorithm in PEM fuel cell on-line diagnosis. IEEE Trans Ind Electron 2018:1.
[20] Mao L, Davies B, Jackson L. Application of the sensor selection approach in polymer electrolyte membrane fuel cell prognostics and health management. Energies 2017;10:1511.
[21] Mao L, Jackson L, Dunnett S. Fault diagnosis of practical polymer electrolyte membrane (PEM) fuel cell system with data-driven approaches. Fuel Cell 2017;17:247–58.
[22] Mao L, Jackson L, Davies B. Investigation of PEMFC fault diagnosis with consideration of sensor reliability. Int J Hydrogen Energy 2017. https://doi.org/10.1016/j.ijhydene.2017.11.144.
[23] Pahon E, Steiner NY, Jemei S, Hissel D, Oteguy PM. A signal-based method for fast PEMFC diagnosis. Appl Energy 2016;165:748–58.
[24] Ritzberger D, Jakubek S. Nonlinear data-driven identification of polymer electrolyte membrane fuel cells for diagnostic purposes: a Volterra series approach. J Power Sources 2017;361:144–52.
[25] Mohammadi A, Djerdir A, Steiner NY, Khaburi D. Advanced diagnosis based on temperature and current density distributions in a single PEMFC. Int J Hydrogen Energy 2015;40:15845–55.
[26] Zheng Z, Morando S, Pera MC, Hissel D, Larger L. Brain-inspired computational paradigm dedicated to fault diagnosis of PEM fuel cell stack. Int J Hydrogen Energy 2017;42:5410–25.
[27] Zhao X, Xu L, Li J, Fang C, Ouyang M. Faults diagnosis for PEM fuel cell system based on multi-sensor signals and principle component analysis method. Int J Hydrogen Energy 2017;42:18524–31.
[28] Li Z, Outbib R, Giurgea S, Hissel D, Jemei S. Online implementation of SVM based fault diagnosis strategy for PEMFC systems. Appl Energy 2016;164:284–93.
[29] Benouioua D, Candusso D, Harel F, Oukhellou L. PEMFC stack voltage singularity measurement and fault classification. Int J Hydrogen Energy 2014;39:21631–7.
[30] Benouioua D, Candusso D, Harel F, Oukhellou L. Fuel cell diagnosis method based on multifractal analysis of stack voltage signal. Int J Hydrogen Energy 2014;39:2236–45.
[31] Kim J, Tak Y. Implementation of discrete wavelet transform-based discrimination and state-of-health diagnosis for a polymer electrolyte membrane fuel cell. Int J Hydrogen Energy 2014;39:10664–82.
[32] Ibrahim M, Antoni U, Steiner NY, Jemei S, Kokonendji C. Signal-based diagnostics by wavelet transform for proton exchange membrane fuel cell. Energy Procedia 2015;74:1508–16.
[33] Damour C, Benne M, Grondin-Perez B, Bessafi M, Hissel D. Polymer electrolyte membrane fuel cell fault diagnosis based on empirical mode decomposition. J Power Sources 2015;299:596–603.
[34] Li Z, Outbib R, Hissel D, Giurgea S. Data-driven diagnosis of PEM fuel cell: a comparative study. Control Eng Pract 2014;28:1–12.
[35] Li Z. Data-driven fault diagnosis for PEMFC systems: automatic. Universite D'aix-Marseille; 2014.
[36] Vamsikrishna KM, Dogra DP, Desarkar MS. Computer-vision-assisted palm rehabilitation with supervised learning. IEEE Trans Bio Med Eng 2016;63:991–1001.
[37] Zhang C, Liu Y, Xia Y, Wang X, Lee C. Reliable accent-specific unit generation with discriminative dynamic Gaussian mixture selection for multi-accent Chinese speech recognition. IEEE Trans Audio Speech Lang Process 2013;21:2073–84.
[38] Befekadu GK, Gupta V, Antsaklis PJ. Risk-sensitive control under Markov modulated denial-of-service (DoS) attack strategies. IEEE Trans Autom Control 2015;60:3299–304.
[39] Li B, Hou J, Li X, Nan Y, Nallanathan A, Zhao C. Deep sensing for space-time doubly selective channels: when a primary user is mobile and the channel is flat Rayleigh fading. IEEE Trans Signal Proces 2016;64:3362–75.
[40] Raman R, Sa PK, Majhi B, Bakshi S. Direction estimation for pedestrian monitoring system in smart cities: an HMM based approach. IEEE Access 2016;4:5788–808.
[41] Missaoui O, Frigui H, Gader P. Land-mine detection with ground-penetrating radar using multistream discrete hidden Markov models. IEEE Trans Geosci Remote 2011;49:2080–99.
[42] Luis Alberto M, Riascos, Simoes Marcelo G, Miyagi Paulo E. A Bayesian network fault diagnostic system for proton exchange membrane fuel cells. J Power Sources 2007;165:267–78.
[43] Ghosh AP, Kleiman E, Roitershtein A. Large deviation bounds for functionals of Viterbi paths. IEEE Trans Inform Theory 2011;57:3932–7.
[44] Miguel A, Ortega A, Buera L, Lleida E. Bayesian networks for discrete observation distributions in speech recognition. IEEE Trans Audio Speech Lang Process 2011;19:1476–89.
[45] Sloin A, Burshtein D. Support vector machine training for improved hidden Markov modeling. IEEE Trans Signal Proces 2008;56:172–88.
[46] Xu J, Han J, Nie F, Li X. Re-weighted discriminatively embedded K-means for multi-view clustering. IEEE Trans Image Process 2017;26:3016–27.

[47] Liu H, Wu J, Liu T, Tao D, Fu Y. Spectral ensemble clustering via weighted K-means: theoretical and practical evidence. IEEE Trans Knowl Data Eng 2017;29:1129–43.
[48] Wu W, Peng M. A data mining approach combining K-means clustering with bagging neural network for short-term wind power forecasting. IEEE Internet Things 2017;4:979–86.
[49] Liang H, Chung W, Kuo S. Coding-aided K-means clustering blind transceiver for space shift keying MIMO systems. IEEE Trans Wirel Commun 2016;15:103–15.
[50] Adapa B, Biswas D, Bhardwaj S, Raghuraman S, Acharyya A, Maharatna K. Coordinate rotation-based low complexity K-means clustering architecture. IEEE Trans VLSI Syst 2017;25:1568–72.
[51] Xing K, Hu C, Yu J, Cheng X, Zhang F. Mutual privacy preserving K-means clustering in social participatory sensing. IEEE Trans Ind Inform 2017;13:2066–76.
[52] Yang X, Xi W, Sun Y, Zeng T, Long T, Sarkar TK. Optimization of subarray partition for large planar phased array radar based on weighted K-means clustering method. IEEE J-STSP 2015;9:1460–8.
[53] Wu XJ, Ye Q. Fault diagnosis and prognostic of solid oxide fuel cells. J Power Sources 2016;321:47–56.